Surface microstructures and corrosion resistance of Ni-Ti-Nb shape memory thin films

Kun Li,[a,b,c] Yan Li,[a,b,*] Xu Huang,[d] Des Gibson,[e] Yang Zheng,[a,b] Jiao Liu,[a,b] Lu Sun[a,b] and Yong Qing Fu[c,*]

[a] School of Materials Science and Engineering, Beihang University, Beijing 100191, China

[b] Beijing Key Laboratory for Advanced Functional Materials and Thin Film Technology, Beihang University, Beijing 100191, China

[c] Faculty of Engineering and Environment, Northumbria University, Newcastle Upon Tyne, NE1 8ST, UK

[d] Memry Corporation, Bethel, CT 06801, USA

[e] Institute of Thin Films, Sensors & Imaging, Scottish Universities Physics Alliance, University of the West of Scotland, Paisley, PA1 2BE, UK

Abstract: Ni-Ti-Nb and Ni-Ti shape memory thin films were sputter-deposited onto silicon substrates and annealed at 600ºC for crystallization. X-ray diffraction (XRD) measurements indicated that all of the annealed Ni-Ti-Nb films were composed of crystalline Ni-Ti (Nb) and Nb-rich grains. X-ray photoelectron spectroscopy (XPS) tests showed that the surfaces of Ni-Ti-Nb films were covered with Ti oxides, NiO and Nb_2O_5. The corrosion resistance of the Ni-Ti-Nb films in 3.5 wt. % NaCl solution was investigated using electrochemical tests such as open-circuit potential (OCP) and potentio-dynamic polarization tests. Ni-Ti-Nb films showed higher OCPs, higher corrosion potentials (E_{corr}) and lower corrosion current densities (i_{corr}) than the binary Ni-Ti film, which indicated a better corrosion resistance. The reason may be that Nb additions modified the passive layer on the film surface. The OCPs of Ni-Ti-Nb films increased with further Nb additions, whereas no apparent difference of E_{corr} and i_{corr} was found among the Ni-Ti-Nb films.

Key words: Ni-Ti-Nb, Thin film, Microstructures, Corrosion resistance

---

*Corresponding Authors: Yan Li, E-mail: liyan@buaa.edu.cn Yongqing Fu, E-mail: richard.fu@northumbria.ac.uk

1. Introduction

Ni-Ti based shape memory alloys (SMAs) have received extensive commercial attention owing to their high damping capacity, high working efficiency and sufficient corrosion resistance [1, 2]. Their mechanical and physical properties can be adjusted by adding ternary or even quaternary alloying elements such as Fe, Cu and Pd [3]. Ni-Ti-Nb SMAs are well known for their wide phase transformation hysteresis and extensively used in sealing, fastening devices and pipe joints [4-6].

Micro-actuators play a prominent role in the development of micro-electro-mechanical systems (MEMS) and various shape memory materials have been investigated to fabricate micro-actuators with high efficiency and better performance [7-11]. For MEMS applications, Ni-Ti-based shape memory thin films are good candidates since they could be easily patterned using conventional lithography methods. Micro-actuators based on shape memory thin films generally show increased actuation frequencies, improved mechanical and fatigue properties, and enhanced working outputs per volume compared with their bulk counterparts [12, 13]. To the best of our knowledge, currently Ni-Ti-Nb films have not been frequently reported when compared with binary Ni-Ti films. In our previous work, martensitic transformation behavior of Ni-Ti-Nb shape memory thin films was studied [14]. Results showed that thermal hysteresis of phase transformation decreased to near zero when the Ni-Ti(Nb) grain size was reduced to ~50 nm, which was attributed to the increased volume fraction of grain boundaries, reduced transformation friction and spontaneous lattice distortion [14]. The near zero thermal hysteresis is beneficial to the development of micro-actuators with high actuation frequencies.

Apart from physical and mechanical properties, corrosion resistance remains a key issue considering the applications of Ni-Ti-based shape memory thin films, especially for devices used in a saline environment under external stresses, in which severe stress induced corrosion and cracking can occur. Nb additions to Ni-Ti or Ti-based alloys have been proven effective in improving the corrosion resistance of the alloys by modifying the surface structures of the alloys [15, 16]. Thus, it is believed that the corrosion resistance of Ni-Ti-Nb films might be improved with Nb additions as well. Therefore,

in the present research, Ni-Ti-Nb films with different Nb contents have been prepared and their corrosion resistance was studied to compare with the performance of a binary Ni-Ti film.

2. Experimental

2.1 Film deposition

Ni-Ti-Nb films were deposited onto Si (100) substrates using a carousel type magnetron sputter as shown in Fig. 1 [17]. An equiatomic Ni-Ti target and a pure Nb target were chosen and placed parallel to each other. The substrates were attached on the rotating drum between the two sputter targets without external heating.

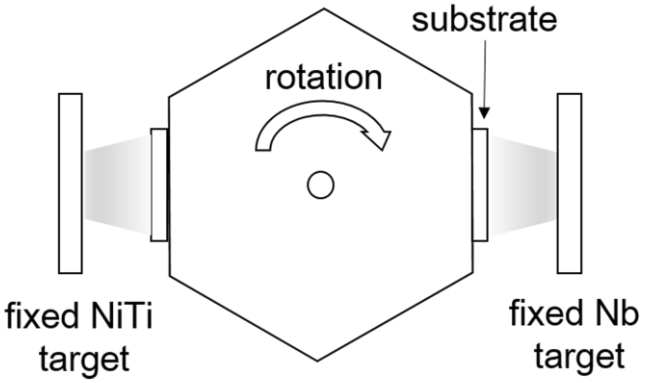

Fig. 1 The schematic image of the carousel type magnetron sputtering equipment (top view).

In order to investigate the composition effect on the corrosion behavior of Ni-Ti-Nb films, the DC power of Ni-Ti target was kept at 400 W whereas that of Nb target was set at 50, 70 and 130 W, respectively. For an easy comparison, samples with different Nb sputtering powers of 50, 70 and 130 W were assigned with names of Nb1, Nb2 and Nb3, respectively. The film thickness was controlled at ~2 μm. The substrates were cleaned using biased plasma and the targets were pre-sputtered with the shutter closed for about 15 minutes. The base pressure was 2×10^{-3} Pa and the working pressure was 0.6 Pa. After deposition, the films were sealed in quartz tubes with a base vacuum of

10^{-5} Pa and annealed at 600ºC for 30 min to achieve a complete crystallization. A Ti-rich Ni-Ti target with a nominal composition of $Ni_{47}Ti_{53}$ was chosen for the deposition of the binary Ni-Ti film for comparison, with the other deposition and annealing parameters the same as those of the Ni-Ti-Nb films.

2.2 Film characterizations

A SmartLab X-ray diffraction (XRD) machine with Cu Kα (λ=1.54056Å) was employed to characterize the crystalline structures of the films. The surface morphology of the annealed films was studied using an atomic force microscope (AFM) under a contact mode at 25ºC, with the scanning area of 1 μm × 1 μm. The compositions of the films were obtained using energy dispersive spectrometry (EDS) with an acceleration voltage of 20 kV. X-ray photoelectron spectroscopy (XPS, K-Alpha, Thermo Scientific) was used to characterize the chemical states of various elements on the film surface with Al Kα monochromatic X-ray source (1486.6 eV) and an Ar ion gun. The survey spectra in the range of 0–1000 eV were recorded for each Ni-Ti-Nb sample and related high-resolution spectra were used to assess the chemical states and concentrations for Ti 2p, Ni 2p and Nb 3d [18]. The spectra were calibrated using the C 1s line (Bonding Energy = 284.6 eV) of the adsorbed hydrocarbon on the surface [19].

The corrosion behavior of the films was characterized using various methods including open circuit potential (OCP) and potentio-dynamic polarization tests [20]. A CHI660E electrochemical work-station was employed for the measurement and a conventional three-electrode system was chosen for all the electrochemistry tests. A platinum electrode was used as the counter electrode and a saturated calomel electrode (SCE) was chosen as the reference electrode. Ni-Ti and Ni-Ti-Nb films were connected to the working electrodes and the edges were sealed using silicone rubber. The surface areas of the working electrodes were controlled to be 10 × 10 mm^2. The electrochemical tests were conducted in 3.5 wt. % NaCl solution at 25ºC. The open circuit potentials of the samples were monitored up to one hour until reaching a steady value. After the OCP tests, potentio-dynamic polarization tests were conducted by scanning from -500 mV to 500 mV vs. OCP, with a scan rate of 1 mV/s.

3. Results and discussion

3.1 Structural and morphological characteristics of the films

The XRD results of all the Ni-Ti and Ni-Ti-Nb films are shown in Fig. 2.

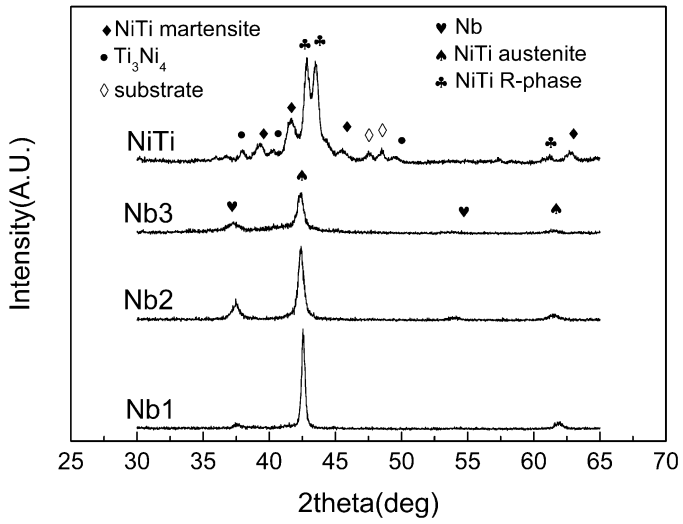

Fig. 2 The XRD curves of the Nb1, Nb2, Nb3 and NiTi samples.

It indicates that all the samples are fully crystallized and are composed of Ni-Ti(Nb) phase (Ni-Ti matrix with a limited Nb solution) and Nb-rich phase (the undissolved Nb with a limited Ni-Ti solution). The peaks at about 2θ=42.7° and 62° correspond to Ni-Ti austenite phase, whereas those at about 2θ=37.5° and 54.1° indicate the existence of Nb-rich phase. The deviation of the measured data from the standard data can be attributed to the solution of Nb atoms in the Ni-Ti matrix [21]. The XRD profile of the Ni-Ti film suggests the existence of R-phase, Ni-Ti martensite and minor amount of Ti_3Ni_4. XRD results indicate that the phase transformation temperatures of the Ni-Ti films are near room temperature, whereas those of Ni-Ti-Nb films are far below room temperature [14].

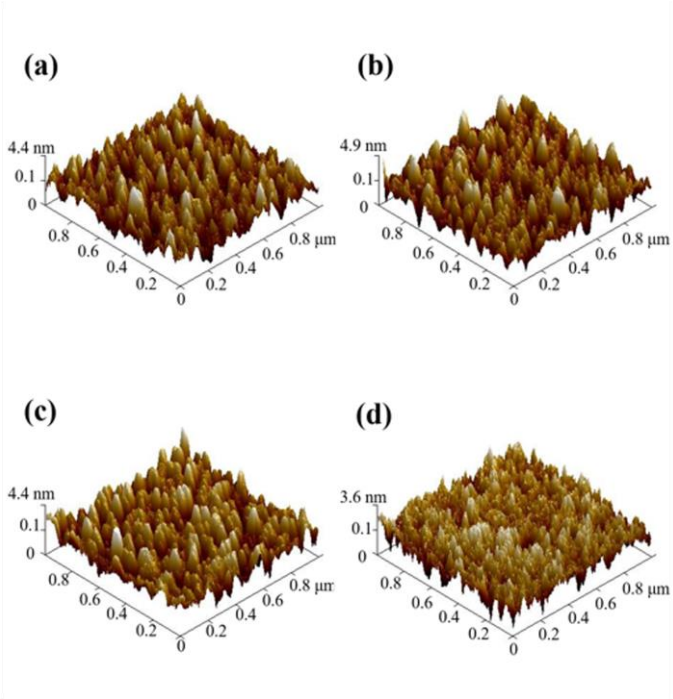

Fig. 3 The AFM images of the (a) Nb1, (b) Nb2 and (c) Nb3 and (d) NiTi samples.

The AFM images of the Ni-Ti, Nb1, Nb2 and Nb3 samples are shown in Fig. 3. The surfaces of all the samples are smooth with nanocrystalline structures. The average roughness (R_a) readings of the Ni-Ti, Nb1, Nb2 and Nb3 samples are 0.78 nm, 1.03 nm, 1.06 nm and 1.00 nm, respectively. The results indicate that there are no apparent differences among the surface roughness of all the samples.

3.2 Compositional and surface characteristics of the films

The compositions of the Ni-Ti and Ni-Ti-Nb films obtained from EDS analysis are listed in Table 1. The results suggest that by increasing the power of the Nb target, the increment in Nb content is unequally shared by the decreases of Ti and Ni contents. The decrease in Ti is more significant than that of Ni, which originates from the higher deposition rate of Ti element than Ni.

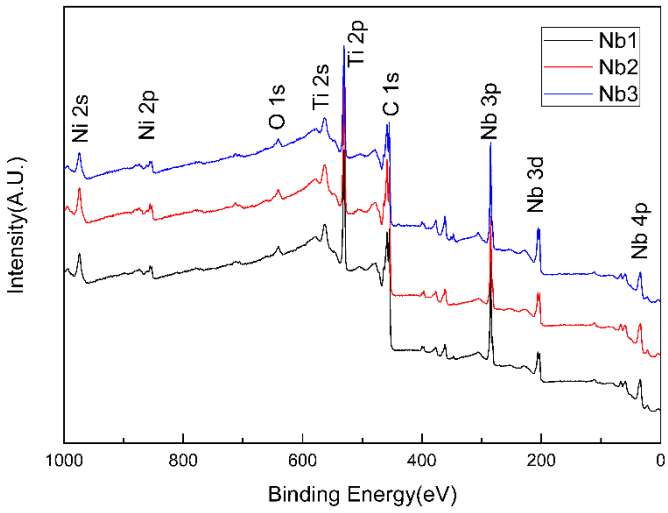

Fig. 4 XPS survey spectrum of the Nb1, Nb2 and Nb3 samples.

Fig. 4 shows the XPS survey spectra obtained from the film surfaces of the Nb1, Nb2 and Nb3 samples. The surface compositions of different samples are listed in Table 2. There are five different elements at the surface of each film, which can be interpreted primarily as the oxides of the metallic elements and carbon contamination. In addition, Ti concentration is considerably higher than those of Ni and Nb in each sample on the film surface.

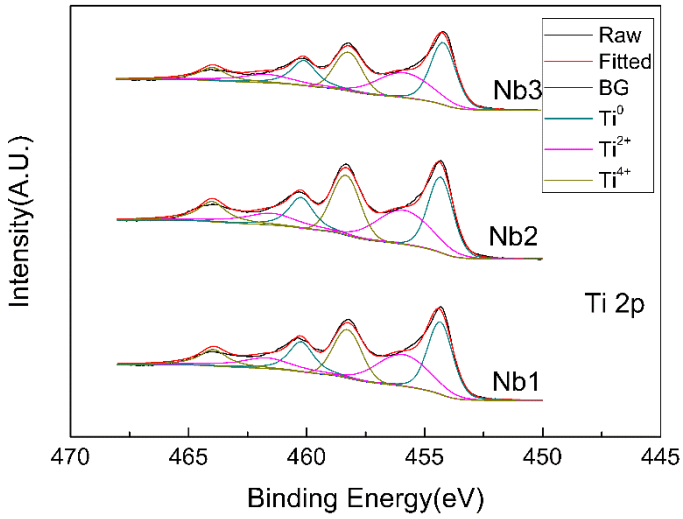

Fig. 5 Gaussian-Lorentzian deconvoluted high resolution spectrum for Ti 2p of the Nb1, Nb2 and Nb3 samples.

Fig. 5 shows the Ti 2p high resolution spectra of Nb1, Nb2 and Nb3 samples. It is obvious that titanium bonds in TiO_2 (464.6 eV and 458.3 eV), TiO (461.7 eV and 455.3 eV) and Ti(Ni) metallic (460.5 eV and 454.3 eV) co-exist in all the samples. Similarly,

Fig. 6 shows the Ni 2p high resolution spectra of Nb1, Nb2 and Nb3 samples, and Fig. 7 shows the Nb 3d high resolution spectra of Nb1, Nb2 and Nb3 samples, respectively. It is obvious that NiO (873.8 eV and 855.0 eV), Ni(Ti) metallic (870.0 eV and 852.4 eV), Nb_2O_5 (209.8 eV and 207.1 eV) and Nb metallic (205.7 eV and 202.8 eV) exist in all the samples [22]. The estimated relative percentages of metallic components and oxides are summarized in Table 3 which is based on the Gaussian-Lorentzian deconvolution of the high resolution spectra. From Table 3, it is suggested that as Nb metallic increases, the content of niobium oxide (Nb_2O_5) decreases, whereas there are less Ti and Ni metallic components in sample Nb2 than in Nb1 and Nb3, with their oxides showing the reverse trends. Compared with the XPS results of Ni-Ti films in reference [13], the difference between the Ni-Ti-Nb films and Ni-Ti films is the existence of Nb_2O_5, which may play a key role in the corrosion behavior of the Nb-containing films.

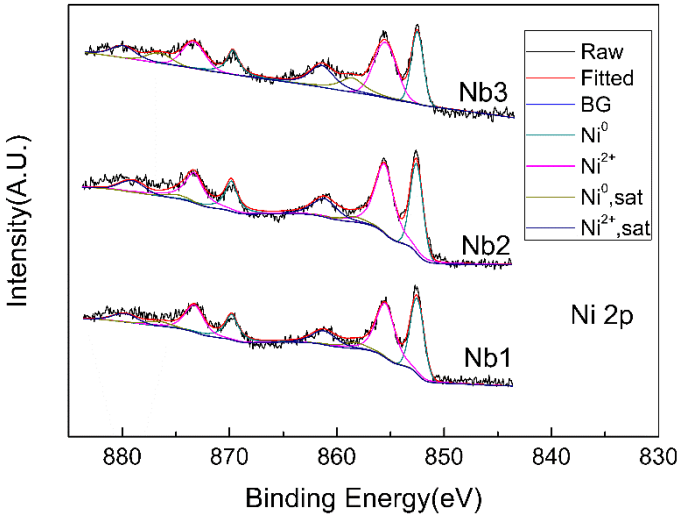

Fig. 6 Gaussian-Lorentzian deconvoluted high resolution spectrum for Ni 2p of the Nb1, Nb2 and Nb3 samples.

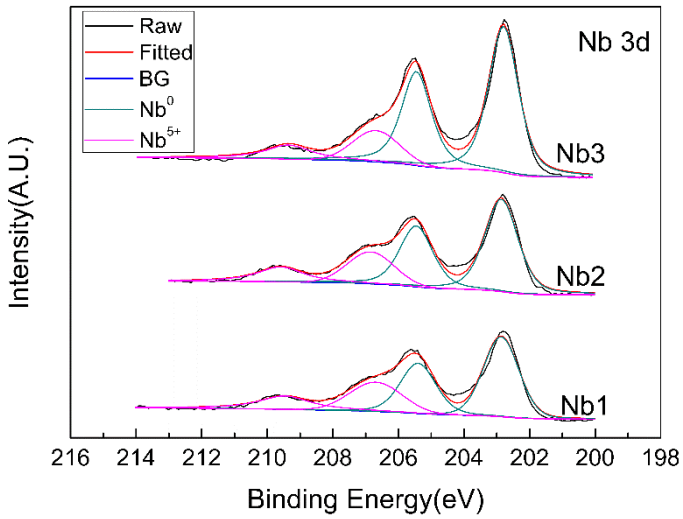

Fig. 7 Gaussian-Lorentzian deconvoluted high resolution spectrum for Nb 3d of the Nb1, Nb2 and Nb3 samples.

3.3 Electrochemical characteristics of the films

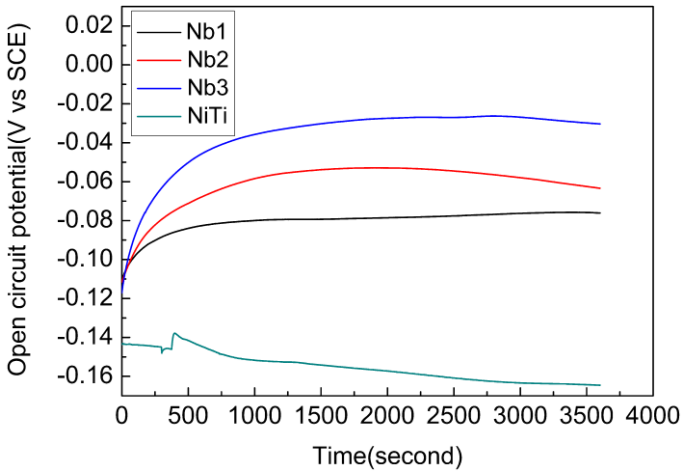

Fig. 8 The open circuit potential as a function of time of the Nb1, Nb2, Nb3 and NiTi samples in 3.5 wt. % NaCl solution at 25°C.

Fig. 8 shows the OCPs as a function of time of the Nb1, Nb2, Nb3 and Ni-Ti samples in 3.5 wt. % NaCl solution at 25ºC. The steady values of OCPs of the samples are listed in Table 4. A general trend can be obtained from Fig. 8 that the OCPs of the Ni-Ti-Nb films increase as the Nb content increases, whereas the OCP of the Ni-Ti sample is much lower. A higher OCP indicate the formation of a thicker passivation layer whereas a decreased potential value shows the dissolution of the passive layer [23]. Different re-passivation and dissolution rates of the hybrid oxides result in the various trends of OCP [24, 25]. All the Ni-Ti-Nb samples have higher OCPs compared

to that of the Ni-Ti film, which indicates that the Ni-Ti-Nb surface states are more chemically stable. This phenomenon has been proven in reference [22], in which T. Zhao et al. investigated the corrosion resistance of Ni-Ti alloys after Nb implantation and found a hybrid oxide layer which consists of TiO_2 and Nb_2O_5, forms on the surface of Ni-Ti alloy. Electrochemical tests show that Nb implantation improves the corrosion behavior of the Ni-Ti alloy by modifying the microstructures of the surface oxide layer. As the Nb content increases, the corresponding OCP also increases, which indicates that Ni-Ti-Nb films with higher Nb contents have more stable corrosion resistance than those with lower Nb contents and are less likely to be corroded from the view of thermodynamics.

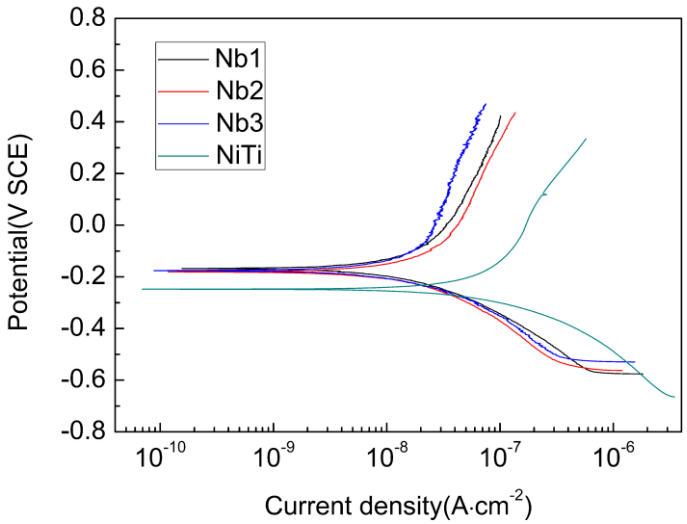

Fig. 9 The potentio-dynamic polarization curves of the Nb1, Nb2, Nb3 and NiTi samples in 3.5 wt. % NaCl solution at 25°C.

The potentio-dynamic polarization curves of the Nb1, Nb2, Nb3 and Ni-Ti samples in 3.5 wt. % NaCl solution at 25ºC are shown in Fig. 9. The corresponding corrosion potential (E_{corr}) and corrosion current density (i_{corr}) of each sample are listed in Table 4. The corrosion potentials for the four samples are different from their corresponding OCPs due to the incomplete stabilization of the passive layer that is formed on the surface of the samples and the cathodic polarization before the stabilization of OCPs [23]. All the samples show small i_{corr} (nA level), which proves the protective effectiveness of the passive layer. There is no signal of breakdown potential in the Tafel curves which indicates that all the samples show no pitting phenomenon

and have a good resistance to severe corrosion [26, 27]. All the Ni-Ti-Nb samples show higher E_{corr} and lower i_{corr} values than the Ni-Ti film, which suggests that Nb additions have a positive influence on the corrosion resistance of Ni-Ti-Nb films. However, from Table 4 it is clear that samples Nb1, Nb2 and Nb3 show close E_{corr} and i_{corr}(in the same order of magnitude), which indicates that the three samples show similar actual corrosion resistances from the view of dynamics.

The corrosion potentials of the Ni-Ti-Nb films can be influenced by several factors, such as surface oxides and roughness. In the present research, both the Ni-Ti-Nb films and the Ni-Ti film show similar surface roughness, which means that the potential influence of the roughness on their corrosion behavior is insignificant [24]. The variations in the corrosion resistance of different samples can be interpreted as the stabilization effect of the passive layer at the surface of the films, caused by Nb additions. The passive layer with niobium oxide addition shows a low solubility and higher stability. From the view of stoichiometry, the niobium cations intend to reduce the anion vacancies in the crystal lattices and make the passive film on Ni-Ti-Nb films more stoichiometric and stabilized [28], which favors the increased corrosion resistance of the films. As for the influence of further Nb addition to the corrosion resistance of the Ni-Ti-Nb films, the OCP and the potentio-dynamic polarization results show different conclusions. OCP tests favor the positive effect of Nb additions to the corrosion resistance of the samples from the view of thermodynamics, whereas potentio-dynamic polarization results show no obvious variation in the corrosion resistance of the same samples from the view of dynamics. Further investigations are needed to interpret the different results and find appropriate theoretical explanations.

4. Conclusions

Ni-Ti-Nb and Ni-Ti thin films have been prepared by sputter deposition. All the four films investigated show a close average roughness. The surfaces of the Ni-Ti-Nb films are covered with a composite oxide layer that consists of titanium oxides, NiO and Nb_2O_5. The Ni-Ti-Nb films exhibit higher open circuit potentials and corrosion potentials as well as lower corrosion current densities compared with the Ni-Ti film. These results indicate that Nb additions can improve the corrosion resistance of Ni-Ti

film by stabilizing the passive film on the film surface. Ni-Ti-Nb films with various Nb contents show little differences in corrosion potentials and corrosion current densities, although the samples with less Nb contents show lower OCPs.

Acknowledgment: Funding supports from UK Engineering Physics and Science Research Council (EPSRC EP/P018998/1), Newton Mobility Grant (IE161019) through Royal Society, and Royal academy of Engineering UK-Research Exchange with China and India are acknowledged. We thank National EPSRC XPS Users' Service (NEXUS), Newcastle University for helping in XPS analysis.

References

[1] A. Bansiddhi, T. D. Sargeant, S. I. Stupp and D. C. Dunand, Porous NiTi for bone implants: A review, Acta Biomater. 4 (2008) 773-782.

[2] S. Shabalovskaya, J. Anderegg and J. Van Humbeeck, Critical overview of Nitinol surfaces and their modifications for medical applications, Acta Biomater. 4 (2008) 447-467.

[3] K. Otsuka and X. Ren, Physical metallurgy of Ti-Ni-based shape memory alloys, Prog. Mater. Sci. 50 (2005) 511-678.

[4] X. M. He, L. J. Rong, D. S. Yan and Y. Y. Li, Temperature memory effect of $Ni_{47}Ti_{44}Nb_9$ wide hysteresis shape memory alloy, Scripta Mater. 53 (2005) 1411-1415.

[5] X. Zhao, X. Yan, Y. Yang and H. Xu, Wide hysteresis NiTi(Nb) shape memory alloys with low Nb content (4.5 at. %), Mater. Sci. Eng., A 438-440 (2006) 575-578.

[6] X. Zhao, J. Xu, L. Tang and S. Gong, High temperature oxidation behavior of NiTiNb intermetallic alloys, Intermetallics 15 (2007) 1105-1115.

[7] Y. Fu, H. Du, W. Huang, S. Zhang and M. Hu, TiNi-based thin films in MEMS applications: a review, Sens. Actuators, A 112 (2004) 395-408.

[8] S. Miyazaki, Y. Q. Fu, W. M. Huang, Thin Film Shape Memory Alloys: Fundamentals and Biomedical Device Applications, Cambridge University Press, 2009, pp. 459.

[9] Y. Q. Fu, S. Sanjabi, Z. H. Barber, T. W. Clyne, W. M. Huang, M. D. Cai, J. K. Luo, A. J. Flewitt, W. I. Milne, Evolution of surface morphology in TiNiCu shape memory thin films, Appl. Phys. Lett. 89 (2006) 171922.

[10] Y. Q. Fu, J. K. Luo, S. E. Ong, S. Zhang, A. J. Flewitt and W. I. Milne, A shape memory microcage of TiNi/DLC films for biological applications, J. Micromech. Microeng. 18 (2008) 035026.

[11] Y. Q. Fu, W. M. Huang, H. J. Du, X. Huang, J. P. Tan and X. Y. Gao, Characterization of TiNi shape-memory alloy thin films for MEMS applications, Surf.

Coat. Technol. 145 (2001) 107-112.

[12] C. Chluba, W. Ge, R. L. Miranda, J. Strobel, L. Kienle, E. Quandt and M. Wuttig, Ultralow-fatigue shape memory alloy films, Science 348 (2015) 1004-1007.

[13] S. K. Sharma and S. Mohan, Influence of annealing on structural, morphological, compositional and surface properties of magnetron sputtered nickel-titanium thin films, Appl. Surf. Sci. 282 (2013) 492-498.

[14] K. Li, Y. Li, K. Y. Yu, C. Liu, D. Gibson, A. Leyland, A. Matthews and Y. Fu, Crystal size induced reduction in thermal hysteresis of Ni-Ti-Nb shape memory thin films, Appl. Phys. Lett. 108 (2016) 171907.

[15] C. Li, Y. F. Zheng and L. C. Zhao, Phase transformation and precipitation in aged Ti-Ni-Hf high-temperature shape memory alloys, Mater. Sci. Eng., A 438-440 (2006) 504-508.

[16] A. K. Shukla, R. Balasubramaniam and S. Bhargava, Properties of passive film formed on CP titanium, Ti-6Al-4V and Ti-13.4Al-29Nb alloys in simulated human body conditions, Intermetallics 13 (2005) 631-637.

[17] A. Ishida and M. Sato, Thickness effect on shape memory behavior of Ti-50.0at. %Ni thin film, Acta Mater. 51 (2003) 5571-5578.

[18] Y. Fu, H. Du, S. Zhang and S. E. Ong, Effect of silicon nitride interlayer on phase transformation and adhesion of TiNi films, Thin Solid Films 476 (2005) 352-357.

[19] Y. Fu, H. Du, S. Zhang and W. Huang, XPS characterization of surface and interfacial structure of sputtered TiNi films on Si substrate, Mater. Sci. Eng., A 403 (2005) 25-31.

[20] N. Bayat, S. Sanjabi and Z. H. Barber, Improvement of corrosion resistance of NiTi sputtered thin films by anodization, Appl. Surf. Sci. 257 (2011) 8493-8499.

[21] J. Li, H. Wang, J. Liu and J. Ruan, Effect of Nb addition on microstructure and mechanical properties of TiNiNb alloys fabricated by elemental powder sintering, Mater. Sci. Eng., A 609 (2014) 235-240.

[22] T. Zhao, Y. Li, Y. Xiang, X. Zhao and T. Zhang, Surface characteristics, nano-indentation and corrosion behavior of Nb implanted NiTi alloy, Surf. Coat. Tech. 205 (2011) 4404-4410.

[23] E. Saebnoori, T. Shahrabi, S. Sanjabi, M. Ghaffari and Z. H. Barber, Surface characteristics and electrochemical behaviour of sputter-deposited NiTi thin film, Philos. Mag. A 95 (2015) 1696-1716.

[24] K. T. Liu and J. G. Duh, Effect of aluminum on the corrosion behavior of NiTiAl thin films, Appl. Surf. Sci. 253 (2007) 5268-5273.

[25] E. X. Sun, S. Fine and W. B. Nowak, Electrochemical behavior of nitinol alloy in Ringer's solution, J. Mater. Sci: Mater. Med. 13 (2002) 959-964.

[26] T. Shahrabi, S. Sanjabi, E. Saebnoori and Z. H. Barber, Extremely high pitting resistance of NiTi shape memory alloy thin film in simulated body fluids, Mater. Lett. 62 (2008) 2791-2794.

[27] K. T. Liu and J. G. Duh, Grain size effects on the corrosion behavior of $Ni_{50.5}Ti_{49.5}$ and $Ni_{45.6}Ti_{49.3}Al_{5.1}$ films, J. Anal. Chem. 618 (2008) 45-52.

[28] M. Metikos-Hukovic, A. Kwodal and J. Piljac, The influence of niobium and vanadium on passivity of titanium-based implants in physiological solution, Biomater. 24 (2003) 3765-3775.

Figure captions:

Fig. 1 The schematic image of the carrousel type magnetron sputtering equipment (top view).

Fig. 2 The XRD curves of the Nb1, Nb2, Nb3 and NiTi samples.

Fig. 3 The AFM images of the (a) Nb1, (b) Nb2 and (c) Nb3 and (d) NiTi samples.

Fig. 4 XPS survey spectrum of the Nb1, Nb2 and Nb3 samples.

Fig. 5 Gaussian-Lorentzian deconvoluted high resolution spectrum for Ti 2p of the Nb1, Nb2 and Nb3 samples.

Fig. 6 Gaussian-Lorentzian deconvoluted high resolution spectrum for Ni 2p of the Nb1, Nb2 and Nb3 samples.

Fig. 7 Gaussian-Lorentzian deconvoluted high resolution spectrum for Nb 3d of the Nb1, Nb2 and Nb3 samples.

Fig. 8 The open circuit potential as a function of time of the Nb1, Nb2, Nb3 and NiTi samples in 3.5 wt. % NaCl solution at 25°C.

Fig. 9 The potentio-dynamic polarization curves of the Nb1, Nb2, Nb3 and NiTi samples in 3.5 wt. % NaCl solution at 25°C.

Table 1 The nominal compositions (at. %) of the Nb1, Nb2, Nb3 and Ni-Ti samples.

Sample	Composition (at. %)
Nb1	$Ti_{42.27}Ni_{48.46}Nb_{9.27}$
Nb2	$Ti_{40.74}Ni_{47.30}Nb_{11.96}$
Nb3	$Ti_{37.02}Ni_{43.68}Nb_{19.30}$
Ni-Ti	$Ti_{48.89}Ni_{51.11}$

Table 2 Surface elemental composition results obtained from XPS spectra of Ni-Ti-Nb films with various Nb contents.

Sample	Ti (at. %)	Ni (at. %)	Nb (at. %)	C (at. %)	O (at. %)
Nb1	15.31	0.79	1.32	55.35	27.23
Nb2	17.42	1.01	1.55	49.63	30.40
Nb3	12.82	0.77	2.12	58.72	25.57

Table 3 The estimated ratios of different chemical states at the surface of the Nb1, Nb2 and Nb3 samples.

Sample	Ti bonds (%)			Ni bonds (%)		Nb bonds (%)	
	Ti	TiO	TiO_2	Ni	NiO	Nb	Nb_2O_5
Nb1	39.8	33.0	27.2	43.0	57.0	66.4	33.6
Nb2	36.4	33.2	30.4	37.3	62.7	71.0	29.0
Nb3	41.8	32.5	25.7	41.0	59.0	78.7	21.3

Table 4 The open circuit potentials (OCP), corrosion potentials and corrosion current densities of the Nb1, Nb2, Nb3 and Ni-Ti samples.

Sample	OCP(V)	E_{corr}(V)	i_{corr}(nA/cm^2)
Nb1	-0.076	-0.168	4.105
Nb2	-0.063	-0.181	7.610
Nb3	-0.030	-0.176	4.129
Ni-Ti	-0.164	-0.245	96.230